Origin of spin-state crossover and electronic reconstruction at the surface of a $LaCoO_3$ nanoparticle

Chao Ma,[1,*] Nan Lin,[1] Zuyong Wang,[1] Shiming Zhou,[2,†] Hongchun Yu,[1] Jiangbo Lu,[3] and Hongwen Huang[1]

[1]*College of Materials Science and Engineering, Hunan University, Changsha 410082, China*

[2]*Hefei National Laboratory for Physical Sciences at the Microscale, University of Science and Technology of China, Anhui 230026, China*

[3]*School of Physics and Information Technology, Shaanxi Normal University, Xi'an 710119, China*

(Received 7 March 2018; revised manuscript received 6 January 2019; published 4 March 2019)

Combining atomic-resolution scanning transmission electron microscopy (STEM) images and electron-energy-loss spectroscopy spectra in aberration-corrected STEM, first-principle calculations, and spectra simulations, we investigate the origin of the surface state in a $LaCoO_3$ nanoparticle. We show that a $LaCoO_3$ nanoparticle appears as the core-shell structure, where the core has the mixture of low- and high-spin states and the shell has increased concentration of the high-spin state. Based on experimental observations and theoretical calculations, we propose that it is neither the oxygen vacancy nor strain but the suppression of oxygen octahedral tilting due to surface reconstruction that plays a dominant role in the spin-state crossover to the higher-spin state at the surface. These results provide great insights into understanding the origin of ferromagnetism as well as the enhanced electrocatalytic activity in this compound.

DOI: 10.1103/PhysRevB.99.115401

I. INTRODUCTION

Surface reconstruction is a ubiquitous phenomenon in the perovskite oxide surface, and would inevitably result in different atomic structure and electronic configuration at the surface from the bulk counterpart [1]. Therefore, to measure atomic and electronic reconstruction at the surface becomes necessary to understand novel surface states and important parameters that govern the surface properties. Recently, the surface state of perovskite cobaltite $LaCoO_3$ has attracted much attention due to its excellent electrocatalytic activity [2,3], which was proposed to be closely correlated with the spin-state transition at the surface. In fact, the $LaCoO_3$ bulk exhibits intriguing magnetic properties, i.e., the spin state can be easily controlled by various factors rather than magnetic field, such as strain [4,5], oxygen vacancy, and lattice distortions [6–9]. In $LaCoO_3$, the specific spin state mainly depends on the competing among Hund exchange energy (Δ_{ex}), crystal-field splitting energy (Δ_{CF}) between t_{2g} and e_g orbitals, and d-orbital valence bandwidth (W). While Δ_{ex} is an intrinsic material constant, both Δ_{CF} and W are easily perturbed through external parameters induced lattice distortions, such as Jahn-Teller distortions and oxygen octahedral rotation [9,10]. Therefore, the structural distortions arising from atomic reconstruction at the surface would lead to changes in the spin state, electronic configuration, and consequently the surface properties.

$LaCoO_3$ bulk exhibits diamagnetic behavior at low temperature, and some Co ions would be thermally excited to higher-spin state above 35 K [11]. However, experimental findings demonstrated that the ferromagnetic ground state can be measured in the strained $LaCoO_3$ film and the surface of $LaCoO_3$ bulk and nanoparticle [12–17]. Although it has been well established that the ferromagnetism in $LaCoO_3$ arises from the transition from the low-spin state ($S = 0$, LS) to intermediate- ($S = 1$, IS) or high-spin state ($S = 2$, HS), the origin of the spin-state transition is still in debate. Due to the complexity of the epitaxial $LaCoO_3$ film, such as epitaxial strains and oxygen vacancy [3,8,18,19], it is still unclear whether the ferromagnetism is due to nonstoichiometry or is an intrinsic feature of the strained $LaCoO_3$ material itself [20,21]. On the other hand, $LaCoO_3$ nanoparticles which show surface ferromagnetism due to surface reconstruction allow us to compare the ferromagnetic shell and diamagnetic core at the same sample, if both structure distortions and electronic structure can be well characterized at the atomic scale. However, to well characterize the atomic and electronic structure at the surface is still challenging, owing to the dominant bulk information over the very weak surface signals. In this paper, using aberration-corrected scanning transmission electron microscopy (STEM) and theoretical calculations, we systematically studied the structure distortions and electronic structure at the surface of a perovskite $LaCoO_3$ nanoparticle. The core-shell structure was well confirmed by both the annular bright-field (ABF) images and electron-energy-loss spectroscopy (EELS) measurements. It was demonstrated that it is the suppression of oxygen octahedral tilting rather than oxygen vacancy that triggers the ferromagnetic surface state in a $LaCoO_3$ nanoparticle.

II. EXPERIMENTAL AND COMPUTATIONAL DETAILS

$LaCoO_3$ nanoparticles were synthesized by a sol-gel method, as reported in Refs. [22] and [23]. STEM images and EELS measurements were performed on a JEOL-ARM200F microscope, operated at 200 kV and equipped with a probe-forming aberration corrector and Gatan image filter

*cma@hnu.edu.cn

†zhousm@ustc.edu.cn

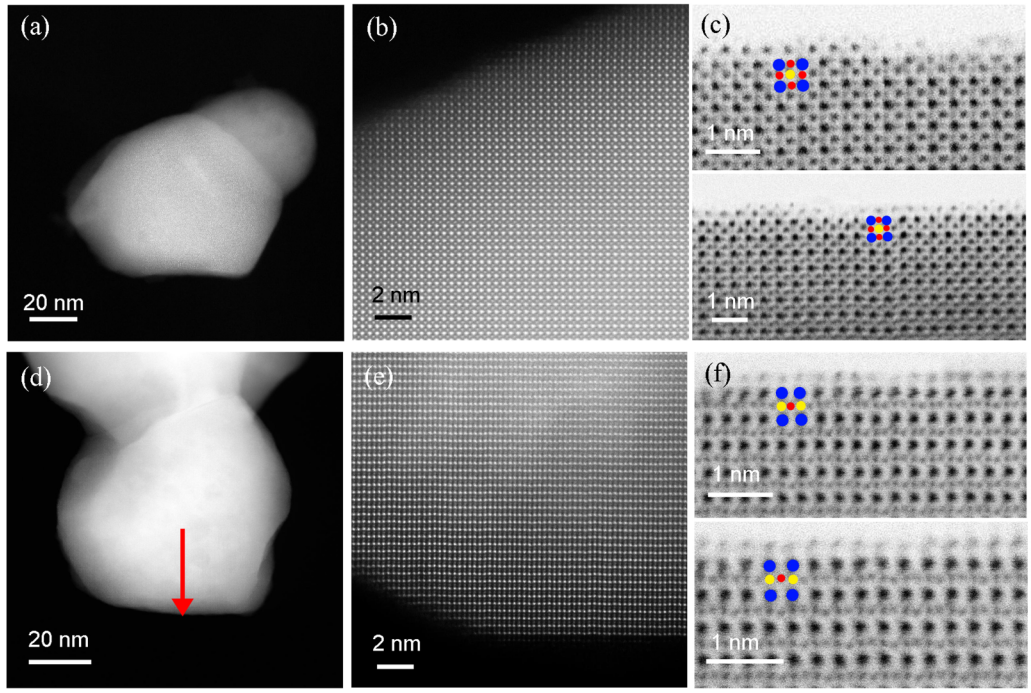

FIG. 1. Aberration-corrected STEM images for $LaCoO_3$ nanoparticles taken along the [2 4 1] (a)–(c) and [2 1 1] (d)–(f) zone axes indexed by the rhombohedral structure. The HAADF-STEM images (a), (b), (d), (e) show the morphology and crystallinity near the edge of the particles. The ABF-STEM images (c), (f) directly display the Co-O terminated surfaces for these nanoparticles. The blue, yellow, and red balls denote the La, Co, and O atoms, respectively.

(Quantum 965). The sample used for TEM characterization was prepared by homogeneously dispersing nanoparticles in ethanol through ultrasonic vibration, and then one drop of such suspensions was put on lacy carbon-covered Cu grid. For high-angle annular dark-field (HAADF) STEM images, the semiconvergence angle is about 24 mrad, and the inner and outer angles of the detector are 90 and 370 mrad, respectively. For the ABF images, the range of collection angle is between 11 and 22 mrad.

First-principle electronic structure calculations were carried out by density-functional theory (DFT) via the WIEN2K code [24], and the O-K-edges spectra simulations are performed by the TELNES program included in the WIEN2K code. The exchange-correlation potential was treated by the local spin-density approximation (LSDA) plus U (LSDA+U, where U is on-site Coulomb interaction). Here, we used $U_{\text{eff}} = U - J$ and $J = 0$, and U_{eff} was set at 4.5 and 8 eV for Co-3d and La-4f orbitals, respectively. The muffin-tin radii R_{mt} were 2.2, 1.9, 1.5 a.u. for La, Co, and O atoms, respectively. The maximum angular momentum of the radial wave functions was set to 10, and $R_{mt}K_{\text{max}}$ was fixed at 7.0 to determine the basis size. Due to the limitation of DFT method to the simulation of L edges of transition-metal element, Co-L-edge EELS spectra were simulated by the charge-transfer multiplet method via CTM4XAS [25]. During the spectra simulations of $Co^{3+}L$ edges by the CTM4XAS program, the Slater integrals were reduced to 80% of their Hartree-Fock values. For CoO_6 cluster, the charge-transfer parameter is set at 2.0 eV, and U_{dd} and U_{cd} are 4.5 and 7 eV, respectively. The crystal-field splitting energies were set to 0, 1, 2, 3, 4, and 5 eV for different spin states.

III. RESULTS AND DISCUSSION

Figure 1 shows STEM images taken from two typical $LaCoO_3$ nanoparticles under different orientations. It was found from the low-magnification HAADF images [Figs. 1(a) and 1(d)] that the diameter is about 70 nm and the particle tends to show certain facets rather than spherical shape. As shown in the high-magnification HAADF images [Figs. 1(b) and 1(e)], the particles exhibit almost perfect lattice fringes, and no defects or oxygen vacancy stripes were found. In addition, it has been reported that the terminated surfaces in perovskite surfaces are closely correlated with the magnetism as well as the catalytic activity. In our experiments, both ABF images taken from [2 1 1] [Fig. 1(c)] and [2 4 1] [Fig. 1(f)] zone axes directly show Co-O terminated surfaces, in good agreement with the proposal by photoemission spectra [16].

Since the surface reconstruction occurs only in several atomic layers, we made full use of atomic-resolution EELS spectra to investigate the electronic structure of the surface. As shown in Fig. 2, the spectra taken from the nanoparticle center are almost the same as those reported for $LaCoO_3$ bulk [26,27], but both O K [Fig. 2(a)] and Co $L_{2,3}$ [Fig. 2(b)] edges taken from the surface region are much different from those from the center region, including peak intensities and energies. In the O K edges [Fig. 2(c)], prepeak a shows decreased intensity and peak b shifts towards lower energy near the surface. The L_3 peak in Co L_3 edges [Fig. 2(d)] also shifts towards lower energy near the surface. Both EELS and x-ray absorption spectroscopy measurements have demonstrated that the prepeak a at around 530 eV in the O K edges is closely correlated to the spin configuration of $LaCoO_3$,

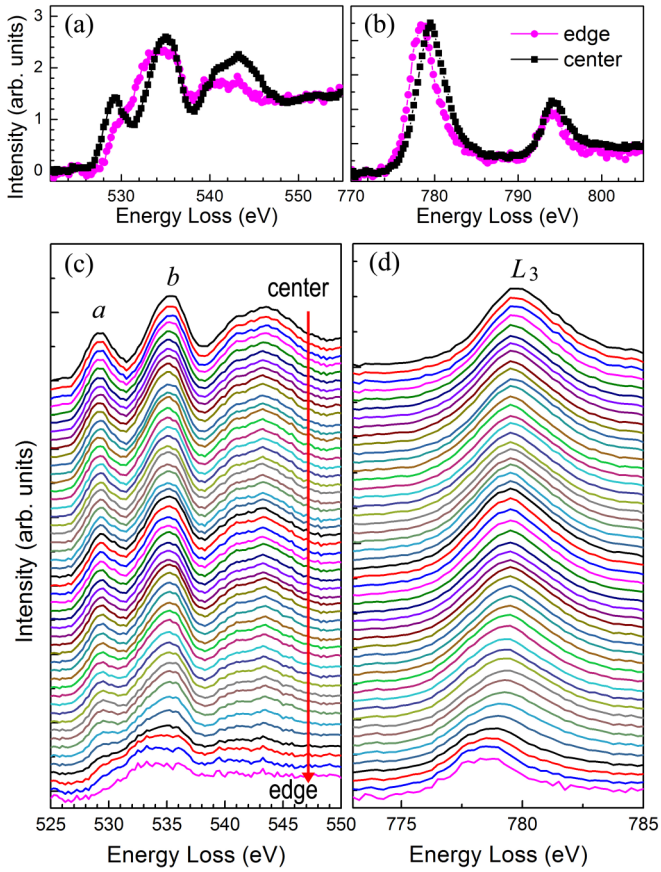

FIG. 2. EELS spectra recorded from a $LaCoO_3$ nanoparticle. (a), (b) O K (a) and Co $L_{2,3}$ (b) edges taken from the center (magenta) and edge (black) of the nanoparticle. (c), (d) A series of O K (c) and Co L_3 (d) edges taken through line scanning from the center to the edge of the nanoparticle, as indicated by the red arrow in Fig. 1(d).

i.e., the higher-spin state shows lower prepeak intensity, as reported in the previous papers [18,19,27–30]. Therefore, these experimental findings definitely suggest a surface state which is much different from the bulk state.

In order to further confirm the distribution of the surface state, both surface and bulk states were mapped in the two-dimensional real space by using the multiple linear least-squares (MLLS) fitting, as shown in Fig. 3(a). It was clearly seen that the surface state only appears very near the nanoparticle edge, forming a core-shell structure in which the core is encapsulated by the shell with different electronic state. From the intensity profiles [Fig. 3(b)] integrated along the direction parallel to the surface, the shell thickness (t_s) is estimated to be 3.5 nm, which is in good agreement with that measured by scanning superconducting quantum interference device microscopy [14].

It was well known that the fine structures in EELS spectra are closely correlated with the electronic structure in transition-metal oxides [31]. For Co $L_{2,3}$ edges which originate from the excitations from the inner $2p$ to unoccupied $3d$ orbitals, both the energy onset of L_3 peak and the white-line branching ratio [$I_3/(I_2+I_3)$, where the I_2 and I_3 are the integrated intensity of L_2 and L_3 peaks] are sensitive to many factors such as oxidation state and spin state. Firstly, we consider the effect of oxidation state which depends on the oxygen content. Figure 3(c) shows the dependence of O:Co atomic ratio on the distance away from the nanoparticle edge. Unlike the notable interface as observed in Fig. 3(b), the atomic ratio remains almost constant except for the outmost layer. The slight reduction at $d > 7$ nm arises from the measuring error due to the increased thickness around the nanoparticle center, while the increased ratio at the outmost layer likely arises from Co cations vacancy or the chemisorption of oxygen, as reported in previous literature [12,14]. Therefore, the used $LaCoO_3$ nanoparticle should be stoichiometric, and the oxidation state of Co ions in the surface region would be identical to that in the center. This phenomenon is quite different from the ferromagnetic $LaCoO_3$ film in which the presence of oxygen vacancy is proposed to play a critical role [18].

Although the oxygen concentration is uniform in the whole nanoparticle, the Co $L_{2,3}$ edges show obvious chemical shift, as shown in Fig. 3(d), in which the L_3 peak shifts towards lower energy nearby the nanoparticle edge. Therefore, such chemical shift would originate from the different spin states. In addition, for transition-metal elements, the changes in the local magnetic moment can be well characterized by the branching ratio of the white line [32,33]. As shown in Fig. 3(e), the branching ratio shows obvious increase near the nanoparticle edge, indicating an increase in magnetic moment. As indicated by the dashed green line, a notable interface can be found around $d = 3.5$ nm, in good agreement with the MLLS fitting [Fig. 3(b)]. Therefore, both chemical shift and branching ratio undoubtedly suggest a spin-state transition towards the higher-spin state at the surface. In $LaCoO_3$, the spin state is sensitive to the e_g-t_{2g} gap (Δ), where $\Delta = \Delta_{CF} - W/2$ [10]. For diamagnetic Co^{3+}, the t_{2g} orbitals are fully occupied and the e_g orbitals are empty. During the spin-state transition, there exists electron hopping from the t_{2g} to e_g orbitals, leading to an increase in magnetic moment. That is, there are more e_g electrons in the magnetic state than those in the diamagnetic state. Therefore, an increase in e_g electrons means the reduction in the e_g-t_{2g} gap, and the Co-e_g band would move downwards, leading to the shift of Co L edge towards lower energy. That is why the L_3 peak shifts towards lower energy even when the oxidation state is not changed. The changes in the occupancy of e_g orbitals can be also found in the O K edges. As shown in Fig. 3(f), the intensity of prepeak a, which is proportional to the holes in e_g orbitals hybridized strongly with O-$2p$ orbitals, shows a notable decrease near the nanoparticle edge, indicating an increase in e_g electrons and the resultant higher-spin state in the surface region.

To further confirm the higher-spin state in the surface region, we performed spectra simulations for O K edges by DFT method and Co L edges by charge-transfer multiplet model. Here, the experimental rhombohedral structure (R-$3c$) was used in the DFT calculations. Although the outmost layer is much different from the bulk, the inner atomic layers in the shell would have the similar symmetry to the bulk. In addition, the previous x-ray diffraction (XRD) measurements have confirmed the rhombohedral structure (R-$3c$) for a $LaCoO_3$ nanoparticle [13,17,22], and the obtained atomic-resolution STEM images and corresponding fast Fourier transform

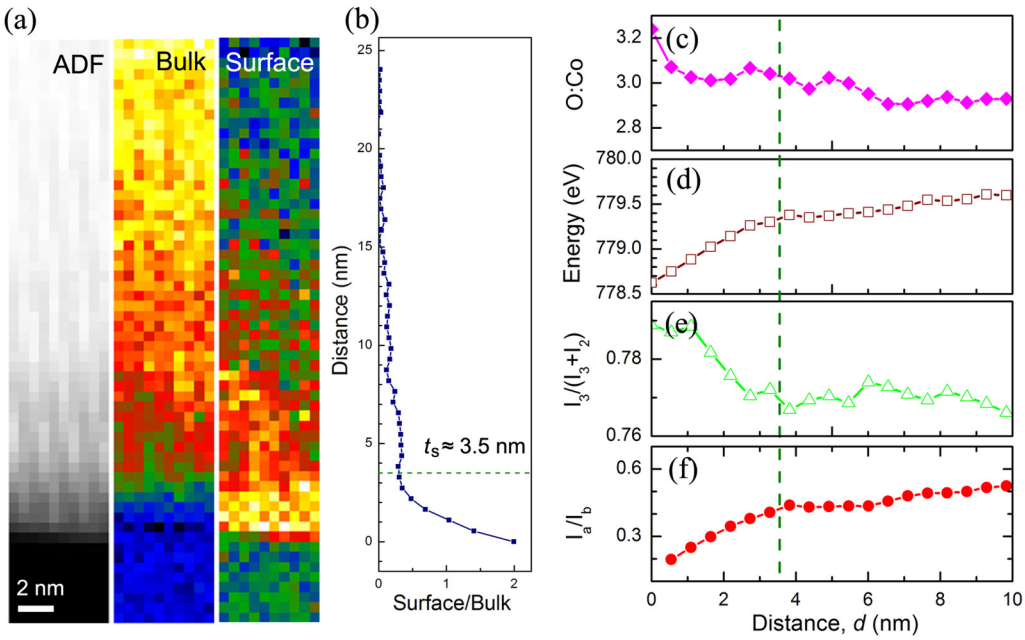

FIG. 3. (a) ADF image (left) and the distribution of the bulk state (middle) and surface state (right) using the MLLS fitting of O K edges. (b) The intensity ratio between the surface and bulk states. (c) The atomic ratio of O and Co atoms as a function of the distance away from the particle edge. (d)–(f) The distance dependence of the L_3 peak energy (c), branching ratio $I_3/(I_2+I_3)$ for Co-L-edges spectra (d), and the intensity ratio of peaks a and b in O K edges (e). The dashed green line denotes the interface separating the core and shell.

patterns which are taken along various sample orientations did not show any symmetry mismatch between the core and shell. Therefore, the shell would have the same symmetry as the core but have different lattice distortions and surface stress due to surface reconstruction. This case is different from the epitaxial film in which the symmetry may be changed due to the symmetry mismatch between the substrate and film.

Figure 4(a) displays the simulated O-K-edge spectra for different spin states, including LS, IS, HS, and various mixed states. It is clear that the higher the spin state, the lower the intensity of prepeak a, i.e., the HS state has the lowest prepeak a. By comparing the experimental O K edges with the simulated ones, the higher-spin state in the shell can be further confirmed. The experimental spectrum taken from the nanoparticle center can be well reproduced by the mixture of LS and HS states with specific LS/HS ratio, confirming the mixed spin state for $LaCoO_3$ bulk at room temperature. As shown in Fig. 4, the simulated spectrum from the IS state is similar to that from the mixture of HS and LS states with the ratio 1:1 (HS+LS), but different from the experimental one (Fig. 2). The spectrum from the mixture of LS, IS, and HS states is very similar to the spectrum from the IS state. Although the mixture of IS and HS states also shows similar spectrum features to the experimental spectrum, this mixed state was not supported by the theoretical calculations [8,34,35]. In fact, the spin state for the bulk at room temperature is still in debate. Both the IS and mixed LS/HS states have been predicted from theoretical calculations, but more and more experimental measurements supported the mixed LS/HS picture [36–41]. Based on our experimental and simulated results, we argued that the mixed state of LS and HS is probably the stable state. Of course, the IS state cannot be completely ruled out, and the confirmation of the mixed LS/HS state still needs more experimental evidence. In addition, according to the continuous changes in the prepeak intensity, the inner layers in the shell under room temperature should be also in the mixture of HS and LS state rather than the pure HS state, and the concentration of the HS state would gradually increase near the particle edge. The good agreement between the simulated O K edges from the HS state and the experimental one taken from the particle edge suggests the HS state at the outmost layer of the nanoparticle.

Due to the large core-hole effect for L edges of transition-metal elements, the DFT method based on one-electron approximation is difficult to reproduce the experimental spectra. Therefore, the charge-transfer multiplet method was used to calculate the Co $L_{2,3}$ edges. In order to probe the relationship between the Co $L_{2,3}$ edges and spin states, the spin states were tuned as a function of the e_g-t_{2g} gap, $\Delta = \Delta_{CF} - W/2$, where W remained constant and only Δ_{CF} was changed. Therefore, a decrease in crystal-field splitting would lead to a decrease in the e_g-t_{2g} gap and in turn the increased local magnetic moment, i.e., higher-spin state [42]. As shown in Fig. 4(b), when the crystal-field splitting energy is decreased, the Co $L_{2,3}$ edges shift towards lower energy. That is, the larger the local magnetic moment, the lower the energy of L_3 peak. This fact well supports our argument that the chemical shift observed in experimental Co $L_{2,3}$ edges originates from different spin states. In addition, it was found that a decrease in the crystal-field splitting results in an increase in branching ratio, in consistence with the relationship between magnetic moment and branching ratio [33]. Therefore, both O K and Co $L_{2,3}$ edges suggest the higher-spin state in the shell. It was also found that the HS and LS crossing point is estimated to be at $\Delta_{CF} = 2.1$ eV, similar to the previously reported value [43].

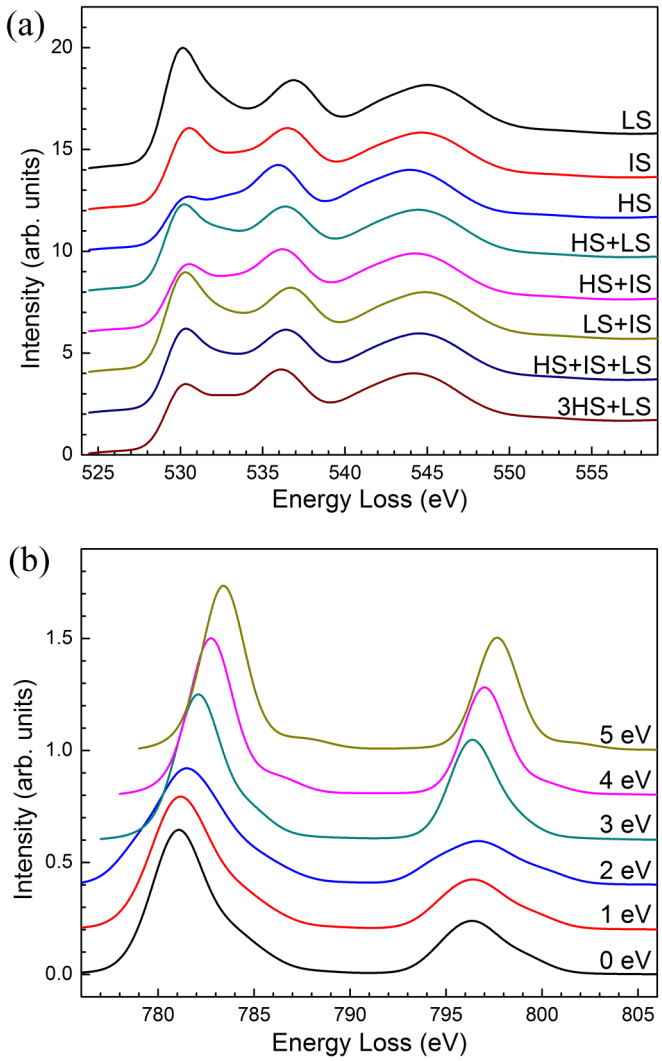

FIG. 4. (a) Simulated O *K* edges by DFT method for different spin states. (b) Simulated Co $L_{2,3}$ edges by the charge-transfer multiplet method for different crystal-field splitting energies (10 Dq).

As discussed above, the higher-spin state in the surface arises from the reduced e_g-t_{2g} gap which depends on lattice distortions due to surface reconstruction. Here, atomic-resolution STEM images were used to reveal the microstructural properties, such as lattice strain and oxygen octahedral tilting. Through the quantitative analysis for the atomic-resolution HAADF-STEM images (Fig. 1), it was found that the surface region has almost the same lattice spacing as the center region. Because of the measurement error, there may exist small lattice strains due to the surface reconstruction. Although a $LaCoO_3$ nanoparticle shows lattice expansion, as demonstrated by XRD measurements [13,44], the strains generated by lattice expansion (<0.2%) are much smaller than that in the epitaxial film (≈2% for $SrTiO_3$ substrate). On the other hand, the previous theoretical calculations predicted that a 2.5% tensile strain is necessary [45], while experimental findings demonstrated that about 1.0% tensile strain is enough to trigger the spin-state transition [7,46]. In our STEM observations (Fig. 1), the lattice expansion in the shell is much smaller than 1.0% and almost undetectable, so the surface lattice expansion would not play a dominant role in the observed spin-state crossover in a $LaCoO_3$ nanoparticle.

Another kind of structural distortion which is closely correlated with the magnetic ordering is the oxygen octahedral tilting, as reported by previous theoretical calculations and experiments [7,10,47]. Thanks to the aberration-corrected ABF image in which heavy La and Co atoms and light O atoms can be all imaged in one single image, we are able to measure quantitatively the oxygen octahedral tilting and distortions [48–50]. The rhombohedral structure of the space group *R*-3*c* is transformed from cubic structure with oxygen octahedral rotation/tilting mode, $a^-a^-a^-$, that is, the $a^-a^-c^0$ tilting angle is equal to the $a^0a^0c^-$ rotation angle. For the $a^0a^0c^-$ rotation, it is almost impossible to measure the rotation angle from ABF-STEM images taken along the [0 0 1] direction (indexed by pseudocubic structure), because of the opposite displacement of oxygen atoms in the adjacent layers. Since the $a^0a^0c^-$ rotation angle is the same as the $a^-a^-c^0$ tilting angle for the rhombohedral structure, we only need to measure the $a^-a^-c^0$ tilting angle. Here, the $a^-a^-c^0$ tilting angle can be measured from the ABF-STEM images taken along the [1 1 0] direction (indexed by the pseudocubic structure) which corresponds to the [2 1 1] direction in the rhombohedral structure. Figure 5(a) shows the dependence of octahedral tilting on the distance away from the nanoparticle edge. It was found that the tilting angle remains constant in the center region but shows obvious reduction near the surface. The thickness of the surface region ($t_s \approx 3.5$ nm) estimated from tilting angle is quite consistent with that from EELS spectra. Therefore, we believe that the spin-state transition deduced from EELS spectra is closely correlated with the change in octahedral tilting. The suppression of oxygen octahedral tilting leads to the increased *d*-orbital bandwidth and consequently the reduced e_g-t_{2g} gap in favor of the higher-spin state, and thus the surface shows the higher-spin state than the nanoparticle center.

Due to small strain and uniform oxygen concentration at the surface region, the suppression of oxygen octahedral tilting would be dominantly controlled by the surface reconstruction [12,16]. Both ABF and HAADF images demonstrated that $LaCoO_3$ nanoparticles show Co-O terminated surface, as shown in Fig. 5 and Fig. 1 in which the Co columns do not show notable displacements but the oxygen columns become blurred at the outmost layer. That is, the dangling bonds lead to the rearrangement of oxygen at the outmost layer, and thus the corresponding oxygen octahedral tilting would be much different from that in the bulk. The suppression of the outmost octahedral tilting would influence the octahedral tilting at the subsurface layer and propagate to several unit cells, similar to the oxygen octahedral coupling at the interface of oxide heterostructures [51]. In addition, the suppressed octahedral tilting is usually accompanied with the lattice expansion, so small surface strain would be expected, as discussed above.

In order to further understand the relationship between the spin state and oxygen octahedral tilting, we performed DFT calculations using the fixed-spin-moment method. Figure 5(b) shows the Co–O–Co bonding angle dependence of total energy for $LaCoO_3$ at different magnetic states, i.e., diamagnetic LS ($S = 0$) and ferromagnetic IS states ($S = 1$), where large Co–O–Co bonding angle corresponds to small

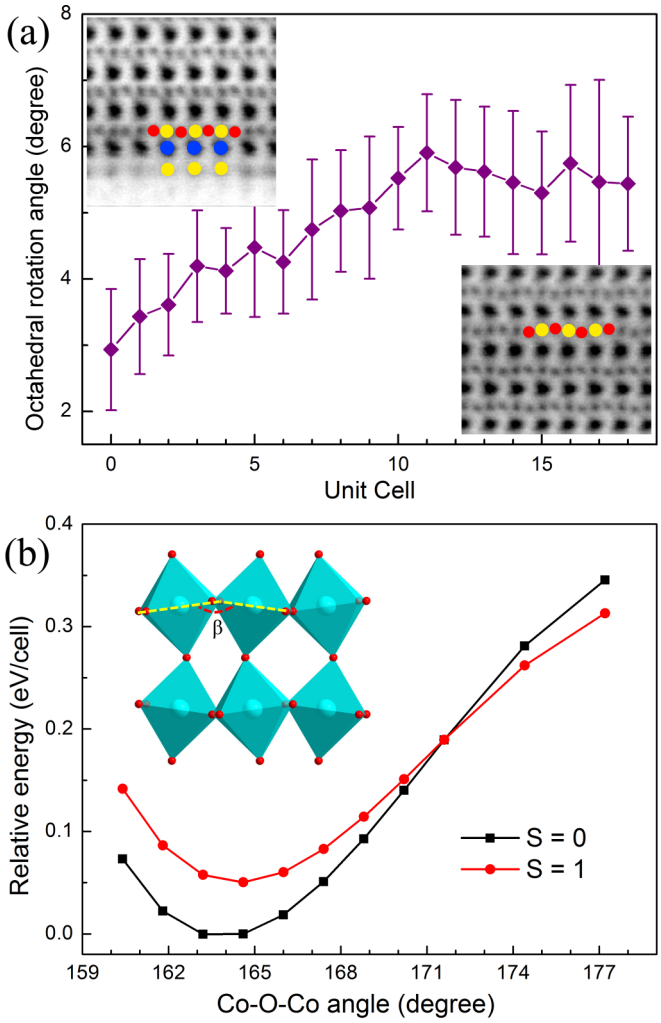

FIG. 5. (a) Oxygen octahedral tilting angle as a function of the distance away from the nanoparticle edge. The insets show the ABF images taken from the nanoparticle edge (top left) and center (bottom right). The yellow, red, and blue balls denote the Co, O, and La atoms, respectively. (b) Calculated total energy for different spin states as a function of Co–O–Co bonding angle. The inset displays the structure model with oxygen octahedral tilting ($a^-a^-c^0$), showing its relationship with the bonding angle β.

oxygen octahedral tilting angle. Because the calculated total energy of the HS state is much larger than that of LS and IS states, the energy curve for the HS state is not shown here. It was found that the LS state is the favorable state for the bulk material at $\beta \approx 164°$. It must be noted that the electronic state obtained by the DFT calculations corresponds to the ground state at zero temperature rather than the real electronic state at room temperature. That is why the EELS spectra taken from the center of a nanoparticle indicate a mixture of HS and LS states. When the oxygen octahedral tilting is suppressed, that is, the Co–O–Co bonding angle is increased, the energy difference between the diamagnetic and ferromagnetic states becomes more and more small, and the total energy of the diamagnetic state becomes higher than that of the ferromagnetic state at $\beta > 171.5°$. That means the ferromagnetic state would become the favorable state at large Co–O–Co bonding angle [16]. According to our STEM observations, this IS state at the surface would be thermally excited to the mixture of LS and HS state under room temperature with the higher concentration of HS state than that in the bulk [52]. Usually, the spin-state crossover is proposed to be driven by the strain, and it was predicted by theoretical calculations and experimental findings that in $LaCoO_3$ the strain-drive spin-state transition occurs at the crossing point of 1.0–2.5% tensile strain [7,45,46]. Therefore, in a $LaCoO_3$ nanoparticle, it is not the tiny strain but the suppression of oxygen octahedral tilting that is mainly responsible for the appearance of the higher-spin state in the surface. In addition, the increased Co–O–Co bonding angle would result in strong hybridization between Co $3d$ and O $2p$ orbitals which is favorable for the higher-spin state and ferromagnetic superexchange interaction [7,45]. This result well explains the observed higher-spin state and ferromagnetism in the shell.

IV. CONCLUSION

In summary, using atomic-resolution EELS measurements and spectra simulations, it was found that in a $LaCoO_3$ nanoparticle, the surface region with a thickness of about 3.5 nm exhibits higher-spin state than the center, forming a core-shell structure at room temperature. The ABF images combined with the theoretical calculations demonstrate that the spin-state crossover originates from mainly the suppression of oxygen octahedral tilting in the surface induced by surface reconstruction. Here, the oxygen vacancy and tensile strain, which are proposed to play a critical role in the ferromagnetic epitaxial $LaCoO_3$ film, hardly contribute to the increased population of HS state at the surface of nanoparticle. These findings not only provide rich information about the surface reconstruction in perovskite cobaltite, but also offer great insights into understanding the origin of ferromagnetism in this compound.

ACKNOWLEDGMENTS

This work was supported by the National Natural Science Foundation of China (Grants No. 11574281 and No. 51501143), Anhui Provincial Natural Science Foundation (Grant No. 1608085MA18), and the Fundamental Research Funds for the Central Universities.

[1] G. Zhu, G. Radtke, and G. A. Botton, Nature (London) **490**, 384 (2012).

[2] J. Suntivich, K. J. May, H. A. Gasteiger, J. B. Goodenough, and Y. Shao-Horn, Science **334**, 1383 (2011).

[3] S. Zhou, X. Miao, X. Zhao, C. Ma, Y. Qiu, Z. Hu, J. Zhao, L. Shi, and J. Zeng, Nat. Commun. **7**, 11510 (2016).

[4] W. S. Choi, J.-H. Kwon, H. Jeen, J. E. Hamann-Borrero, A. Radi, S. Macke, R. Sutarto, F. He, G. A. Sawatzky, V. Hinkov, M. Kim, and H. N. Lee, Nano Lett. **12**, 4966 (2012).

[5] D. Fuchs, C. Pinta, T. Schwarz, P. Schweiss, P. Nagel, S. Schuppler, R. Schneider, M. Merz, G. Roth, and H. v. Löhneysen, Phys. Rev. B **75**, 144402 (2007).

[6] K. Gupta and P. Mahadevan, Phys. Rev. B **79**, 020406(R) (2009).

[7] D. Fuchs, E. Arac, C. Pinta, S. Schuppler, R. Schneider, and H. v. Löhneysen, Phys. Rev. B **77**, 014434 (2008).

[8] J. M. Rondinelli and N. A. Spaldin, Phys. Rev. B **79**, 054409 (2009).

[9] L. Qiao, J. H. Jang, D. J. Singh, Z. Gai, H. Xiao, A. Mehta, R. K. Vasudevan, A. Tselev, Z. Feng, H. Zhou, S. Li, W. Prellier, X. Zu, Z. Liu, A. Borisevich, A. P. Baddorf, and M. D. Biegalski, Nano Lett. **15**, 4677 (2015).

[10] G. E. Sterbinsky, P. J. Ryan, J.-W. Kim, E. Karapetrova, J. X. Ma, J. Shi, and J. C. Woicik, Phys. Rev. B **85**, 020403(R) (2012).

[11] J.-Q. Yan, J.-S. Zhou, and J. B. Goodenough, Phys. Rev. B **69**, 134409 (2004).

[12] J.-Q. Yan, J.-S. Zhou, and J. B. Goodenough, Phys. Rev. B **70**, 014402 (2004).

[13] I. Fita, V. Markovich, D. Mogilyansky, R. Puzniak, A. Wisniewski, L. Titelman, L. Vradman, M. Herskowitz, V. N. Varyukhin, and G. Gorodetsky, Phys. Rev. B **77**, 224421 (2008).

[14] A. Harada, T. Taniyama, Y. Takeuchi, T. Sato, T. Kyômen, and M. Itoh, Phys. Rev. B **75**, 184426 (2007).

[15] Z. Zhang, Ultramicroscopy **107**, 598 (2007).

[16] S. Halilov, E. Gorelov, M. Izquierdo, A. Yaroslavtsev, V. Aristov, P. Moras, P. M. Sheverdyaeva, S. K. Mahatha, F. Roth, A. Lichtenstein, and S. L. Molodtsov, Phys. Rev. B **96**, 205144 (2017).

[17] A. M. Durand, D. P. Belanger, T. J. Hamil, F. Ye, S. Chi, J. A. Fernandez-Baca, C. H. Booth, Y. Abdollahian, and M. Bhat, J. Phys.: Condens. Matter **27**, 176003 (2015).

[18] N. Biškup, J. Salafranca, V. Mehta, M. P. Oxley, Y. Suzuki, S. J. Pennycook, S. T. Pantelides, and M. Varela, Phys. Rev. Lett. **112**, 087202 (2014).

[19] V. V. Mehta, N. Biskup, C. Jenkins, E. Arenholz, M. Varela, and Y. Suzuki, Phys. Rev. B **91**, 144418 (2015).

[20] Q. Q. Lan, X. Shen, H. W. Yang, H. R. Zhang, J. Zhang, X. X. Guan, Y. Yao, Y. G. Wang, R. C. Yu, Y. Peng, and J. R. Sun, Appl. Phys. Lett. **107**, 242404 (2015).

[21] J.-H. Kwon, W. S. Choi, Y.-K. Kwon, R. Jung, J.-M. Zuo, H. N. Lee, and M. Kim, Chem. Mater. **26**, 2496 (2014).

[22] S. Zhou, L. Shi, J. Zhao, L. He, H. Yang, and S. Zhang, Phys. Rev. B **76**, 172407 (2007).

[23] S. Zhou, L. He, S. Zhao, Y. Guo, J. Zhao, and L. Shi, J. Phys. Chem. C **113**, 13522 (2009).

[24] P. Blaha, K. Schwarz, G. Madsen, D. Kvasnicka, and J. Luitz, *WIEN2K, An Augmented Plane Wave + Local Orbital Program for Calculating Crystal Properties* (Karlheinz Schwarz, Technical University, Wien, Austria).

[25] E. Stavitski and F. M. F. de Groot, Micron **41**, 687 (2010).

[26] A. Gulec, D. Phelan, C. Leighton, and R. F. Klie, ACS Nano **10**, 938 (2016).

[27] R. F. Klie, J. C. Zheng, Y. Zhu, M. Varela, J. Wu, and C. Leighton, Phys. Rev. Lett. **99**, 047203 (2007).

[28] J. Gazquez, W. Luo, M. P. Oxley, M. Prange, M. A. Torija, M. Sharma, C. Leighton, S. T. Pantelides, S. J. Pennycook, and M. Varela, Nano Lett. **11**, 973 (2011).

[29] M. W. Haverkort, Z. Hu, J. C. Cezar, T. Burnus, H. Hartmann, M. Reuther, C. Zobel, T. Lorenz, A. Tanaka, N. B. Brookes, H. H. Hsieh, H.-J. Lin, C. T. Chen, and L. H. Tjeng, Phys. Rev. Lett. **97**, 176405 (2006).

[30] Q. Q. Lan, X. J. Zhang, X. Shen, H. W. Yang, H. R. Zhang, X. X. Guan, W. Wang, Y. Yao, Y. G. Wang, Y. Peng, B. G. Liu, J. R. Sun, and R. C. Yu, Phys. Rev. Mater. **1**, 024403 (2017).

[31] H. Tan, J. Verbeeck, A. Abakumov, and G. V. Tendeloo, Ultramicroscopy **116**, 24 (2012).

[32] F. M. F. de Groot, J. Electron. Spectrosc. Relat. Phenom. **67**, 529 (1994).

[33] D. M. Pease, A. Fasihuddin, M. Daniel, and J. I. Budnick, Ultramicroscopy **88**, 1 (2001).

[34] H. Hsu, P. Blaha, and R. M. Wentzcovitch, Phys. Rev. B **85**, 140404(R) (2012).

[35] H. Hsu, P. Blaha, R. M. Wentzcovitch, and C. Leighton, Phys. Rev. B **82**, 100406(R) (2010).

[36] K. Asai, A. Yoneda, O. Yokokura, J. M. Tranquada, G. Shirane, and K. Kohn, J. Phys. Soc. Jpn. **67**, 290 (1998).

[37] P. M. Raccah and J. B. Goodenough, Phys. Rev. **155**, 932 (1967).

[38] J. B. Goodenough, J. Phys. Chem. Solids **6**, 287 (1958).

[39] D. Meng, H. Guo, Z. Cui, C. Ma, J. Zhao, J. Lu, H. Xu, Z. Wang, X. Hu, Z. Fu, R. Peng, J. Guo, X. Zhai, G. J. Brown, R. Knize, and Y. Lu, Proc. Natl. Acad. Sci. USA **115**, 2873 (2018).

[40] K. Knížek, Z. Jirák, J. Hejtmánek, P. Novák, and W. Ku, Phys. Rev. B **79**, 014430 (2009).

[41] K. Tomiyasu, J. Okamoto, H. Y. Huang, Z. Y. Chen, E. P. Sinaga, W. B. Wu, Y. Y. Chu, A. Singh, R.-P. Wang, F. M. F. de Groot, A. Chainani, S. Ishihara, C. T. Chen, and D. J. Huang, Phys. Rev. Lett. **119**, 196402 (2017).

[42] J.-S. Zhou, J.-Q. Yan, and J. B. Goodenough, Phys. Rev. B **71**, 220103(R) (2005).

[43] F. Guillou, Q. Zhang, Z. Hu, C. Y. Kuo, Y. Y. Chin, H. J. Lin, C. T. Chen, A. Tanaka, L. H. Tjeng, and V. Hardy, Phys. Rev. B **87**, 115114 (2013).

[44] P. M. Diehm, P. Agoston, and K. Albe, ChemPhysChem **13**, 2443 (2012).

[45] H. Seo, A. Posadas, and A. A. Demkov, Phys. Rev. B **86**, 014430 (2012).

[46] Y. Yokoyama, Y. Yamasaki, M. Taguchi, Y. Hirata, K. Takubo, J. Miyawaki, Y. Harada, D. Asakura, J. Fujioka, M. Nakamura, H. Daimon, M. Kawasaki, Y. Tokura, and H. Wadati, Phys. Rev. Lett. **120**, 206402 (2018).

[47] A. M. Durand, D. P. Belanger, C. H. Booth, F. Ye, S. Chi, J. A. Fernandez-Baca, and M. Bhat, J. Phys.: Condens. Matter **25**, 382203 (2013).

[48] S. D. Findlay, N. Shibata, H. Sawada, E. Okunishi, Y. Kondo, and Y. Ikuhara, Ultramicroscopy **110**, 903 (2010).

[49] C. Ma, Y. Lin, H. Yang, H. Tian, L. Shi, J. Zeng, and J. Li, Adv. Mater. **27**, 6328 (2015).

[50] Q. He, R. Ishikawa, A. R. Lupini, L. Qiao, E. J. Moon, O. Ovchinnikov, S. J. May, M. D. Biegalski, and A. Y. Borisevich, ACS Nano **9**, 8412 (2015).

[51] J. M. Rondinelli, S. J. May, and J. W. Freeland, MRS Bull. **37**, 261 (2012).

[52] B. Chakrabarti, T. Birol, and K. Haule, Phys. Rev. Mater. **1**, 064403 (2017).